

Article

High Purity/Recovery Separation of Propylene from Propyne Using Anion Pillared Metal-Organic Framework: Application of Vacuum Swing Adsorption (VSA)

Majeda Khraisheh ¹, Fares AlMomani ^{1,*} and Gavin Walker ²

¹ Department of Chemical Engineering, College of Engineering, Qatar University, Doha P.O. Box 2713, Qatar; m.khraisheh@qu.edu.qa

² Department of Chemical Sciences, SSPC, Bernal Institute, University of Limerick, V94 T9PX Limerick, Ireland; Gavin.Walker@ul.ie

* Correspondence: falmomani@qu.edu.qa; Tel.: +974-4403-4140

Abstract: Propylene is one of the world's most important basic olefin raw material used in the production of a vast array of polymers and other chemicals. The need for high purity grade of propylene is essential and traditionally achieved by the very energy-intensive cryogenic separation. In this study, a pillared inorganic anion SiF_6^{2-} was used as a highly selective C_3H_4 due to the square grid pyrazine-based structure. Single gas adsorption revealed a very high C_3H_4 uptake value (3.32, 3.12, 2.97 and 2.43 $\text{mmol}\cdot\text{g}^{-1}$ at 300, 320, 340 and 360 K, respectively). The values for propylene for the same temperatures were 2.73, 2.64, 2.31 and 1.84 $\text{mmol}\cdot\text{g}^{-1}$, respectively. Experimental results were obtained for the two gases fitted using Langmuir and Toth models. The former had a varied degree of representation of the system with a better presentation of the adsorption of the propylene compared to the propyne system. The Toth model regression offered a better fit of the experimental data over the entire range of pressures. The representation and fitting of the models are important to estimate the energy in the form of the isosteric heats of adsorption (Q_{st}), which were found to be 45 and 30 $\text{kJ}\cdot\text{Kmol}^{-1}$ for propyne and propylene, respectively. A Higher Q_{st} value reveals strong interactions between the solid and the gas. The dynamic breakthrough for binary mixtures of $\text{C}_3\text{H}_4/\text{C}_3\text{H}_6$ (30:70 v/v) were established. Heavier propylene molecules were eluted first from the column compared to the lighter propyne. Vacuum swing adsorption was best suited for the application of strongly bound materials in adsorbents. A six-step cycle was used for the recovery of high purity C_3H_4 and C_3H_6 . The VSA system was tested with respect to changing blowdown time and purge time as well as energy requirements. It was found that the increase in purge time had an appositive effect on C_3H_6 recovery but reduced productivity and recovery. Accordingly, under the experimental conditions used in this study for VSA, the purge time of 600 s was considered a suitable trade-off time for purging. Recovery up to 99%, purity of 98.5% were achieved at a purge time of 600 s. Maximum achieved purity and recovery were 97.4% and 98.5% at 100 s blowdown time. Energy and power consumption varied between 63–70 kWh/ton at the range of purge and blowdown time used. The VSA offers a trade-off and cost-effective technology for the recovery and separation of olefins and paraffin at low pressure and high purity.

Keywords: MOFs; Olefin-Paraffin Separation/paraffin; cryogenic separation; vacuum swing adsorption; pressure swing adsorption; breakthrough curves; Toth model; propylene; propyne



Citation: Khraisheh, M.; AlMomani, F.; Walker, G. High Purity/Recovery Separation of Propylene from Propyne Using Anion Pillared Metal-Organic Framework: Application of Vacuum Swing Adsorption (VSA). *Energies* **2021**, *14*, 609. <https://doi.org/10.3390/en14030609>

Received: 29 September 2020

Accepted: 7 December 2020

Published: 25 January 2021

Publisher's Note: MDPI stays neutral with regard to jurisdictional claims in published maps and institutional affiliations.



Copyright: © 2020 by the authors. Licensee MDPI, Basel, Switzerland. This article is an open access article distributed under the terms and conditions of the Creative Commons Attribution (CC BY) license (<https://creativecommons.org/licenses/by/4.0/>).

1. Introduction

The vast increase and addiction to energy and plastics are expected to rise in the future. Light hydrocarbons ($\text{C}_2\text{-C}_4$) are the most demanded materials for polymer industries around the globe [1]. In specific, C_3H_6 is the second most important and used hydrocarbon in the world after ethylene. It is an intermediate material for a vast array of products such as polyvinyl chloride, polypropylene and most importantly, polyethylene [2].

Cryogenic distillation is the most conventional and industrially used technology for the separation of olefins and paraffin. It is used for example to produce 99.9% purity ethylene from ethylene-ethane mixtures [3–7]. In the case of C_2H_2/C_2H_4 , C_2H_4/C_2H_6 , C_3H_4/C_3H_6 and C_3H_8 system, cryogenic distillation requires a huge number of theoretical plates to achieve a good gas separation and purity. The most challenging and demanding, from economic and energy perspectives, is the separation of C_3H_4 and C_3H_6 [8–12] as the relative volatility of their mixture is very close, resulting in a very large separation column (with upwards of 100 theoretical stages), large reflux ratio and subsequently high operating and energy costs. Steam/catalytic cracking of higher chain hydrocarbons is the main method of producing propylene and inevitably contains amounts of propyne. Propyne (C_3H_4), with concentrations of 1000–2000 ppm, is produced during steam cracking and is considered to be the main impurity that is known to cause poisoning effect of the catalyst during the cracking process with a detrimental effect on the production of propylene [8]. To meet the polymer grade propylene requirements, the content of propyne must be reduced to less than 5 ppm. It is therefore imperative to remove propyne from the propylene gas streams to produce the required propylene polymer required grade gas (>999.99% purity). The separation of propane (C_3H_8) and propylene is well reported in literature given its demanding energy requirements and close relative volatilities of both compounds at the temperature range of 244–327 K [2,13–19]. However, only a few studies have reported the separation of C_3H_4/C_3H_6 mixtures [20–23]. Accordingly, finding technological alternatives to this conventional separation process have been the intense focus of research. In addition, alternatives such as adsorption/distillation hybrids, adsorption, and membrane separation permeation using porous materials like zeolites or metal-organic frameworks (MOFs) were reported [24,25]. Among zeolites, 4A zeolite and 13X zeolite [14,17,26–28] have been intensively reported. MOFs are sometimes referred to as porous coordinated polymer and are tunable materials that consist of multifunctional linkers (organic or inorganic) joining metal nodes. A number of very good reviews on MOFs are available in the literature [24,29,30]. The development of advanced adsorption technologies based on newly developed metal-organic frameworks opens new frontiers separations such as propane/propylene, ethylene/ethane, CO_2/N_2 , CO_2/CH_4 and propylene/propyne [22,31]. However, the separation of propyne and propylene is rarely reported in the literature. Li et al. [21] reported in 2017 on the best performing MOFs for the separation of propyne from propylene. The uptake capacities of ELM-12 were about $2.0 \text{ mmol}\cdot\text{g}^{-1}$ and $0.0025 \text{ mmol}\cdot\text{g}^{-1}$ for $Cu(dhbc)_2(4,4'\text{-bipy})$. In 2018, Yang et al. [12] reported on the use of pillared hybrid ultra-microporous (HUM) SiF_6^{2-} and NbO_5^{2-} as a single molecular trap of C_3H_4 at an ultralow concentration of C_3H_4 in C_3H_6 mixture and recorded a new benchmark for the uptake of C_3H_4 under with a value of $2.0 \text{ mmol}\cdot\text{g}^{-1}$. A suitable separation system is essential for utilization of any sorbent new materials for a specific separation as it will affect the cost, footprint and process efficiency [32–34]. Compared to traditional activated carbon or zeolites, MOFs attracted a vast research focus for many gas separations due to their superior flexibility, tenability and functionality [20,24,25,33,35–42]. Metal-organic frameworks used for olefin separation can be mainly divided into two categories: open metal site MOFs that results in propylene higher equilibrium selectivity and MOFs with size sieving optimal pore aperture (elevated kinetic selectivity to C_3H_6) [43,44]. The ability to control their synthesis, functional surface groups, pore size offers the MOFs a great advantage in targeting specific difficult gas separations. Gases with a clear difference in molecular size, vapour pressures and other properties, such as CO_2/N_2 , CO_2/CH_4 , CO/CO_2 , O_2/N_2 can be separated due to their different interaction with the MOF structure [8,10,12,19,45,46]. Gases with very similar molecular weights and vapor pressures ($C_3H_4/C_3H_6/C_3H_8$) are very difficult to separate using traditional methods. In the case of C_2H_2/C_2H_4 , C_2H_4/C_2H_6 , C_3H_4/C_3H_6 and C_3H_8 system, cryogenic distillation is used with a huge number of theoretical plates to achieve a good gas separation and purity. The most challenging separation is related to C_3H_4 and C_3H_6 . For example, the kinetic diameter difference between C_2H_2 (3.3 Å) and C_2H_4 (4.84 Å) is 0.9 Å. In the case of C_3H_4 (4.2 Å)

and C_3H_6 (4.6 Å) the 0.4 Å small difference in the kinetic diameter can result in a very energy-intensive separation process as suggested by Li et al. [22]. The separation of propylene from propyne requires a material with specific molecular sieving ability an affinity towards propyne over propylene with a high adsorption capacity at ultralow pressures. Such materials are not well available or documented in the literature. Anion pillared HUMs are typically three-dimensional coordinated networks of anions such as Ni, Cu or Zn that are well connected to two-dimensional networks of metal nodes. SiF_6^{2-} (SIFSIX), $NbOF_5^{2-}$ and AlF_5^{2-} are examples of anion pillar materials that form bridges with organic linkers in the MOF structure and are reported to have potential application in gas separations such as C_3H_6/C_3H_8 and other lower alkene/alkane separations. The development of a new class of materials to achieve this particular energy-intensive separation is required.

MOFs distinguish themselves from other porous materials by their modular setup and framework flexibility which offers a strong π -complexations between these metal sites and the olefin molecules which can be advantages in e.g., fixed-bed adsorption applications. Because of the high purity of the olefins needed for polymerization, the desirable high recovery rates and the accompanying energy, time and capital consuming multi-bed/-step separation/purification are required. Two basic steps are required in commercial adsorption: preferential adsorption and regeneration which can be achieved via cyclic adsorption processes such as pressure (PSA) [3,47–50], vacuum (VSA) [51–56] and temperature (TSA) [57]. SA as a stand-alone or hybrid combination has been investigated in different studies [32,51,55,58–60]. In PSA at least four to five beds in 4–6 steps are reported. It can be seen that the applicability and development of effective materials are tightly related to the separation system design, its configuration, and energy requirements. Fixed bed adsorbed configuration are most studies given their simplicity, ease of design and versatile ability to screen a large number of new sorbents compared to fluidized beds. In a typical pressure (vacuum) swing operation pressurization, adsorption, blowdown and purge are the basic benchmark cyclic operation. The rinse stage is also added to ensure a high purity product [61]. Changes to the operational parameters can greatly dictate the purity and recovery of the product.

Using metal-organic frameworks for the specific separation of propyne/propylene is still at the early stages with few reported studies in literature and the studies of propyne/propylene separation on metal-organic frameworks are lacking [22]. No reports have been published on the use of SIFSIX-3-Ni MOF for the separation of propyne/propylene using PSA/VSA or TSA applications. Such studies are essential to assess the performance of the benchmark MOF materials in realistic industrial application settings. The aim is to bridge the gap between material design and real-world engineering applications. In addition, as earlier reports [12] indicate that C_3H_4 and C_3H_6 are strongly absorbed within the MOF structure, VSA application has the advantage of the recovery of such strongly bond gas under sub-atmospheric conditions. Accordingly, in this investigation, the experimental work related to the separation of propyne from propylene mixture is investigated. Firstly, the synthesized MOF is characterized by morphology and pore structure. In addition, single gas adsorption uptake behaviour on the adsorbent was established under various temperatures (300–360 K) and a variety of pressures (10–100 kPa) using Rubotherm manganic balance. Isotherms were fitted to two main isotherms (Langmuir and Toth models). The investigation also considered the kinetic breakthrough for 30:70% (*v/v*) C_3H_4/C_3H_6 gas mixtures in a single fixed-bed column set up. Once the base equilibrium and dynamic behaviour of the single and multi-gas mixtures were established, the VSA system consisting of 6 steps (adsorption, depressurization, rinsing, blowdown, purge and pressurization) was tested. Effect of different operation times of purge and blowdown stages were tested with respect to the product (propylene) purity, recovery and productivity. The energy requirements were established to assess the trade-off conditions required to best operate the system for optimal recovery and separation of propylene.

2. Materials and Methods

All used reagents and chemicals were of analytical grade purity mostly supplied by Sigma-Aldrich. Single pure gases were supplied by Buzwair Inc. Qatar supplied from with

99.99% purity. Synthesis of SIFSIX-3-Ni ($\text{Ni}(\text{pyrazine})_2\text{SiF}_6$) $_n$ -SIFSIX-3-N: SIFSIX-3-Ni is one of the hybrid ultra-microporous class of MOFs reported recently and they combine ultramicropores (<0.7 nm). It is mainly formed from transition metals linked by organic ligands and inorganic anions [62].

(size D1:5.03, D2:3.75, D3:4.6 Å³), is pyrazine-based metal-organic frameworks and was prepared following the method described in earlier work [63,64]. In short 3 mol of $\text{Ni}(\text{NO}_3)_2$, 6 mmol pyr., 3 mmol of $(\text{NH}_4)_2\text{SiF}_6^{2-}$ were dissolved in 4 mL of deionized water and stirred for 2 days. The slurry was then filtered under a vacuum then submerged in methanol for 24 h. The samples were then dried in a convection oven at 150 °C overnight. The resultant blue powder was then degassed to activate the sorbent ahead of experimental work. An illustration showing the linkers and pyrazine is shown in Figure 1.

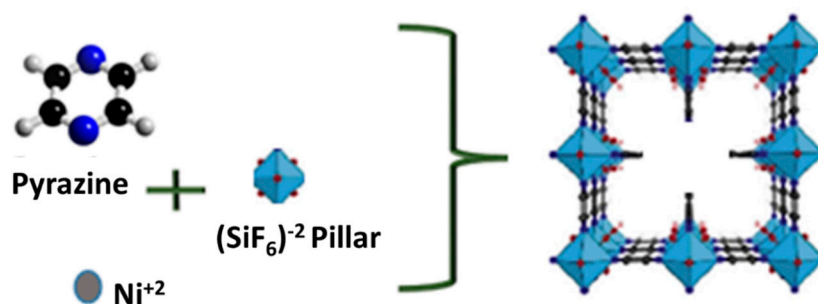


Figure 1. Illustrative structure of SIFSIX-3-Ni.

Morphology and microporosity: Brunauer–Emmett–Teller (BET) analysis were conducted using liquid nitrogen. After 3 h of degassing, the adsorption and desorption under vacuum conditions were conducted at 150 °C. The BET surface area was established and was found to be around 368 ($\text{m}^2 \cdot \text{g}^{-1}$). Pore size and pore volumes were 0.36(nm) and 0.167 ($\text{cm}^3 \cdot \text{g}^{-1}$), respectively. Full experimental details are described in detail in Khraisheh et al. [63].

Powder X-Ray diffraction patterns were collected using Panalytical Empyrean diffractometer. Continuous scanning mode was used ($\text{Cu K}\alpha = 1.54 \text{ \AA}$) with an operating power of 40 Kv and fixed divergence slit of 0.76 mm. Thermogravimetric analysis (TGA) were conducted under N_2 gas. Fourier-transform infrared spectroscopy (FTIR) (using Bruker Vertex 80) for the adsorbents was conducted in the range of 4000–400 cm^{-1} . The SEM analyses were conducted following standard protocols and discussed in detail in Khraisheh et al. [63].

Single pure gas adsorption uptake experiments were conducted using Rubotherm Prazisionsmesstechnik (GmbH, Bochum, Germany). The system was equipped with a magnetic suspension balance (MSB) and integrated gas dosing system (GDS). Adsorption and desorption were facilitated by an automated Teledyne pump (Isco 260D) allowing pressurization and depressurization up to a max 35 MPa. An illustration of the system and its components are shown in Figure S1. The change in temperature and pressure occurs in a stepwise controlled fashion. The system is also equipped with the required pressure transducers and temperature sensors. Ahead of any equilibrium experiments, the system and the sample (typically around 0.1–0.2 g) are evacuated under helium at 400 K for few hours under vacuum conditions until no weight change is detected and the system is assumed to have reached equilibrium. The required operating temperature can also be adjusted and the adsorption isotherms for propylene (propylene) and propyne (propyne) at 300, 320, 340 and 360 K.

The dynamic breakthrough and the vacuum swing uptake adsorption for single and multicomponent gases were conducted using a fixed-bed stainless steel column configuration packed with around 87 g MOF (bed porosity: 0.4; bulk density 389 $\text{kg} \cdot \text{m}^{-3}$) as shown in Figure 2. The vertical column was 0.20 m in diameter and 0.60 m in height. The temperature was controlled by placing the column in a convection oven that facilitates the control of the outside temperature. The gas feed in the column was regulated via flow

controllers. The temperature inside the column was monitored using K-type thermocouples at three different locations alongside the height of the vertical column at 0.15, 0.4 and 0.6 m from the bed inlet side (designating, the bottom, middle and top of the column near-wall respectively). The flow of the gases in and out of the column was regulated using solenoid valves. The required mix of the binary gas was created by controlling the mass flow of the pure gases ahead of the column. Mass flow controllers were used to achieve gas purge (propyne) and rinse (propylene) as indicated in the locations illustrated in Figure 2. Pressure control valves were used to control the column pressure. Gases were analyzed using a gas chromatograph connected to the apparatus. Temperature, pressure and flow rate were recorded using a data acquisition system. Breakthrough isotherms for the single gas were conducted with a 1.2 SLPM (at 100 kPa and 273 K) of a pure gas (propylene or propyne). The bed is initially flooded with helium at 1 SLPM, 340 K and 150 KPa. When equilibrium is attained after each experiment, the column is again degassed with helium without having to change the bed temperature or pressure and to ensure complete degassing and full regeneration of the bed. For binary systems, the breakthrough was also attained using the same conditions but the desired gas feeds were obtained via controlling the mass flow of the pure gases. The molar fraction of propylene to propyne was 30:70% *v/v* at a flow rate of 1.2 SLPM. The adsorption bed itself with the packed solid was heated overnight to 423 K with helium flow ahead of the breakthrough experiments.

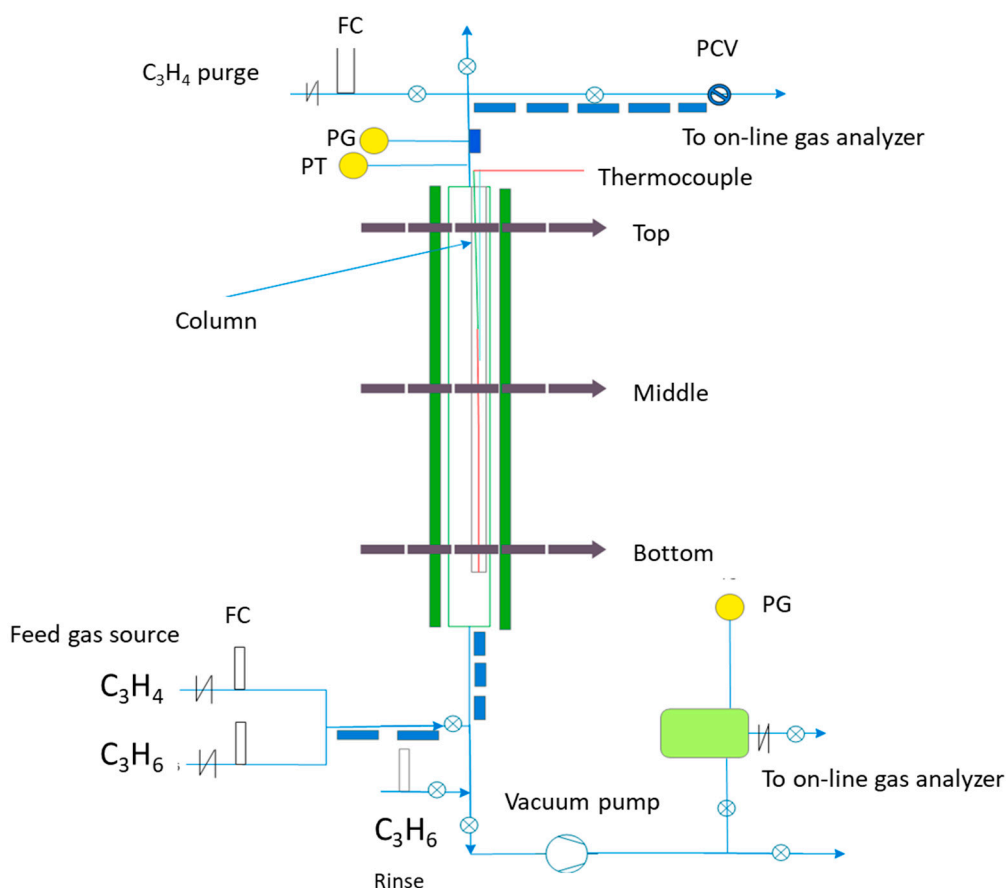


Figure 2. Schematic showing the fixed bed column (Vacuum Pump—Rocker Scientific, New Taipei City, Taiwan, China; Pressure control valve—SS-43GXS4 Swagelok, Solon, Ohio, USA; Mass Flow Controllers Bronkhorst High-Tech B.V, Nijverheidsstraat, The Netherlands).

Vacuum pressure swing (VPS) experiments were conducted to effectively separate a binary 30:70% mixture of propyne and propylene with high propylene purity. The VSP cycle consisted of 5–6 cycles depending on whether propyne recovery is the main goal or

propyne and propylene. If both gases are to be recovered the system will have a rinse step. Similar set-ups were used for the N₂ propylene recovery [49,52] and no-rinse was used for the separation of propane and propylene. Different stages were used in various studies with VSA cycles were formed using four [34,56,65], five [66] or six [49] steps depending on the required purity of the product and the nature of the binary system. The 6 steps cycle of the VSA is then repeated as expressed in S2. The 6 main steps include feed or adsorption, depressurization/rinse, blowdown, purge and pressurization are presented in Figure 3. The depressurization was conducted in the countercurrent operational mode. The experimental conditions in a given VPS cycle are given in Table 1. The first cycle is the feed step into the adsorption column where the gases are introduced at the entrance of the bed. The bed at this step was operated at high pressure (250 kPa). The step is followed by a low-pressure countercurrent depressurization step operated at 100 kPa. To obtain high purity propylene, a rinse step is used and is operated with no change of pressure from the previous step. The propylene is obtained in the blowdown step which operates at low pressure (10 kPa). The purge with propyne is carried out at 10 kPa. The outlet gas stream from this step can be recovered, recycled or purged as a waste product. The pressurization takes place using the propyne product until the bed pressure reaches 250 kPa and the cycle can start again. A trade-off between the low pressure (vacuum) and the purity of the product is required with respect to increased energy costs. In the rinse and purge stages, pure gases were used as required.

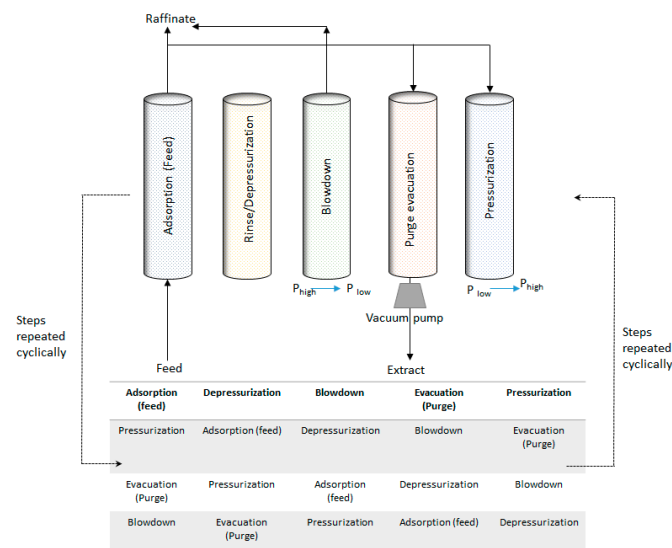


Figure 3. Schematic showing the full VSA cycle configurations used.

Table 1. Experimental operating conditions for typical vacuum pressure swing (VPS) cycles.

Cycle Step	Cycle Time (s)	Pressure (kPa)	Flow Rate (SLPM)	Composition	
				PROPYLENE	PROPYNE
Adsorption	800	250	1.2	0.7	0.30
Depressurization	100	100	-	-	-
Rinse	600	100	1.2	1.0	-
Countercurrent Blowdown	100 (150–250) *	250 down to 10	-	-	-
Low pressure Purge	600	10	1	-	1.0
Countercurrent Pressurization	50	10–250	1.2	-	1.0

* Blowdown time and purge time indicated inside brackets are used to estimate the effect of those two operational modes on purity, recovery and productivity.

3. Results and Discussion

The SEM analysis of the prepared MOF is shown in Figure 4. Powders consisted of multi-sized agglomerations that range from 100–600 nm in size. Smooth and uniform particle shapes were observed with voids present between granules. Small crystal sizes are very desirable in fixed bed applications as they minimize the mass transfer resistance and increase the surface area per volume [66]. The prepared materials were tested to ascertain their bulk purity, identities and crystalline structure using XRD of a set wavelength. A scattering pattern results when a microcrystalline sample is hit by X-Rays, which can be used to characterize the ordering of the crystalline structure. Figure S3 shows the characterization of SISFIX-3-Ni in terms of XRD before and after activation as well as FTIR patterns. It can be seen that XRD was consistent with the reported crystal structure suggesting that the required phase purity was achieved during the experimental preparation with the required synthesized framework. The peak 12.4° at 2θ corresponded to 100 planes in the SIFSIX-3-Ni crystal lattice. The peak is more visible and intense than other peaks. It can be inferred that readily exposed one-dimensional channels are available for the passage of the gas within the SIFSIX-3-Ni.

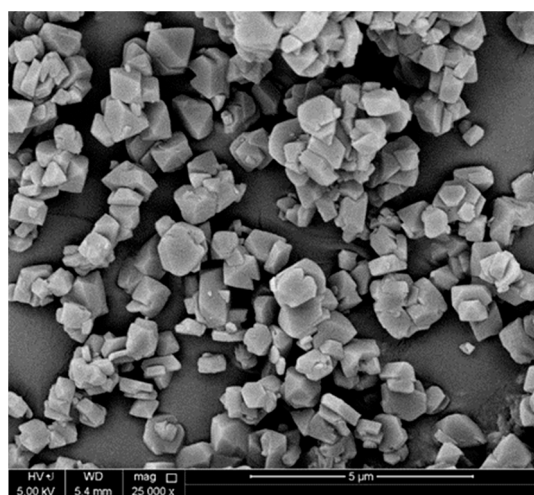


Figure 4. SEM of SIFSIX-3-Ni.

Thermogravimetric analysis TGA was performed to establish the thermal stability of the material. Tests were performed in temperatures reaching 750°C in the presence of nitrogen gas (Figure S4). It can be observed that a steeper change in material weight was observed between $280\text{--}300^\circ\text{C}$, resulting in around 15% decrease in mass. The TGA patterns were in agreement with reported TGAs [43,67,68]. The initial evaporation of water and other volatiles is the most likely reason for the observed initial loss of mass, however, the larger drop in weight of the sample at higher temperature can be attributed to the decomposition of the material and the loss of wall and structural integrity [44,69,70]. Figure S5 shows the N_2 adsorption-desorption isotherm. The shape of the adsorption and desorption isotherms indicated a reversible Type-I isotherm following IUPAC categorization. This typically is indicative of the formation of uniform narrow mesopores and a wider distribution of the pores [69–71]. The initial steep rise in the N_2 adsorption-desorption isotherm at the low relative pressure (P/P_0 less than 0.001) is typically associated with the formation of established microporosity. The high-adsorbed volume values at relative pressures higher than 0.8 are reported to be attributed to the N_2 capillary condensation in the antiparticle pores and indicating a possible expandable pore and a flexible structure which may lead to what is known as the gate-opening effect [9,21,22,72]. The N_2 adsorption-desorption isotherms did not indicate the presence of a clear hysteresis loop at a low P/P_0 ratio. A slight hysteresis effect is present at a higher P/P_0 ratio.

3.1. Adsorption of Pure Compounds on SIFSIX-3-Ni

Pure gas-solid adsorption isotherms were determined for temperatures of 300, 320, 340 and 360 K. The uptake values of the two pure gases on SIFSIX-3-Ni are represented in Figure 5a in $\text{mmol}\cdot\text{g}^{-1}$ at pressures ranging from 1–120 kPa. The isotherm trends of the uptake values vs. the pressures reflects a clear difference in the adsorption ability of the solid towards the two pure gases. That is, the smaller gas molecule of propyne was absorbed faster (steeper curves) and in larger uptake quantities compared to those of propylene in all temperature ranges (300–360 K). The maximum adsorption for propyne were 3.32, 3.12, 2.97 and 2.43 $\text{mmol}\cdot\text{g}^{-1}$ at 300, 320, 340 and 360 K, respectively. The values for propylene for the same temperature range were 2.73, 2.64, 2.31 and 1.84 $\text{mmol}\cdot\text{g}^{-1}$, respectively. Yang et al. [12] reported on the adsorption uptake values using three different types of SIFSIX (SIFSIX1-Cu, SIFSIX-2-Cu-i and SIFSIX-3-Ni). The prepared materials showed steep adsorption at low pressures and temperatures around 298 K. The authors reported that under low pressure and 700 ppm C_3H_4 the recorded maximum adsorption was 2.0 $\text{mmol}\cdot\text{g}^{-1}$ for SIFSIX-3-Ni. In this study, the performance of the prepared SIFSIX MOF is superior when compared to other materials reported in the literature under the current experimental conditions (Table 2). It can also be noted that a steep increase in the adsorption capacity at the lower pressure range is more apparent in the case of propyne and SIFSIX combination at all temperature ranges in comparison with the rest of the adsorbent/adsorbate systems (Figure 5a). In all cases, the adsorption of propyne is higher than that for propylene at all temperature ranges and in both adsorbents. A similar result was reported but, in the propylene, and C_3H_8 systems on different metal-organic frameworks [13]. These higher affinity and uptake values can also be related to the better BET surface area and pore structure of the SIFSIX metal-organic frameworks. The kinetic diameter of the molecule will have a major effect on the selectivity of one gas over another. The linear propyne molecule ($4.16 \times 4.01 \times 6.51 \text{ \AA}$) is smaller than the larger curve-shaped propylene ($4.64 \times 4.16 \times 6.44 \text{ \AA}$) [22]. Besides, the existence of the methyl group in both gases makes their kinetic diameter quite close (4.2 and 4.6 \AA for propyne and propylene, respectively). This small difference in kinetic diameter is one of the main reasons for the difficulty and energy intensity of the separation of the two gases in general and the large number of theoretical stages needed in the traditional cryogenic distillation used for the separation. The micropores analysis of the SIFSIX and kinetic diameter (average 4.2 \AA) will allow both propyne and propylene to enter the pores. Nonetheless, it seems that the availability of a large number of anions (SiF_6^{2-}) in the pores and channels of the framework [22] have a better binding ability for alkynes as compared to alkenes creating a preferred sieving effect towards propyne. The maximum equilibrium adsorption value reported here for the SIFSIX MOF was higher than that reported for the same material and propyne separation (1.87 $\text{mmol}\cdot\text{g}^{-1}$) [22]. The difference may be attributed to the different $v/v\%$ ratios used in the reported study. In addition, the value recorded in our work is similar to the benchmark uptake value reported for UTSA-200 ($[\text{Cu}(\text{azpy})_2(\text{SiF}_6)]_n$; azpy = 4,4'-azopyridine) in the recent work by Li et al. [22]. The main reason for the good reported selectivity is the small aperture size of the UTSA-200 (3.4 \AA) meaning that size exclusion is the only dominating mechanism in this case compared to stronger interactions between SIFSIX and the propyne gas. Yang et al. [12] reported that the precise tuning of the size of the inorganic anion hybrid ultramicroporous materials based on SiF_6^{2-} serves as a single molecule trap towards propyne. The clear difference in the uptake capacity at the same temperature and pressures above 10 kPa between propyne and propylene is indicative of the ability to use this solid to effectively separate the two gases given the adsorption preference and selectivity of the SIFSIX.

Figure 5a depicts as well the profound effect of the temperature on the adsorption of the pure gases. Temperatures in the range of 300–360 K were used for pressures up to 100 kPa. The ability of the material to adsorb the gas decreases (for both gases) with the increase in temperature. The gap between the adsorption uptakes of the solid between the 300–320 K are not as large as those at elevated temperatures (340–360 K). Other adsorption

systems such as propylene and C_3H_8 reported in studies showed similar trends with respect to uptake values vs. temperature [13]. In addition, a study of the adsorption-desorption behaviours for propyne and propylene on SIFSIX (Figure S6) is essential to ascertain the reversibility, hence the release of the gases upon generation. It is also evident that the hysteresis effect is more pronounced in propyne adsorption compared to that for propylene. This indicated a strong affinity and molecular interactions between propyne molecules and the structure of the sorbents. For propylene, a small hysteresis is observed. A similar effect was reported in a recent study by Lin et al. [45] where solids such as SIFSIX-1-Cu, SIFSIX-2-Cu-i, ELM-12 interacted strongly with propyne at pressures less than 20 kPa. These strong interactions were exhibited in a steep adsorption uptake isotherm at a fixed temperature over propylene with reported benchmark uptake values [22].

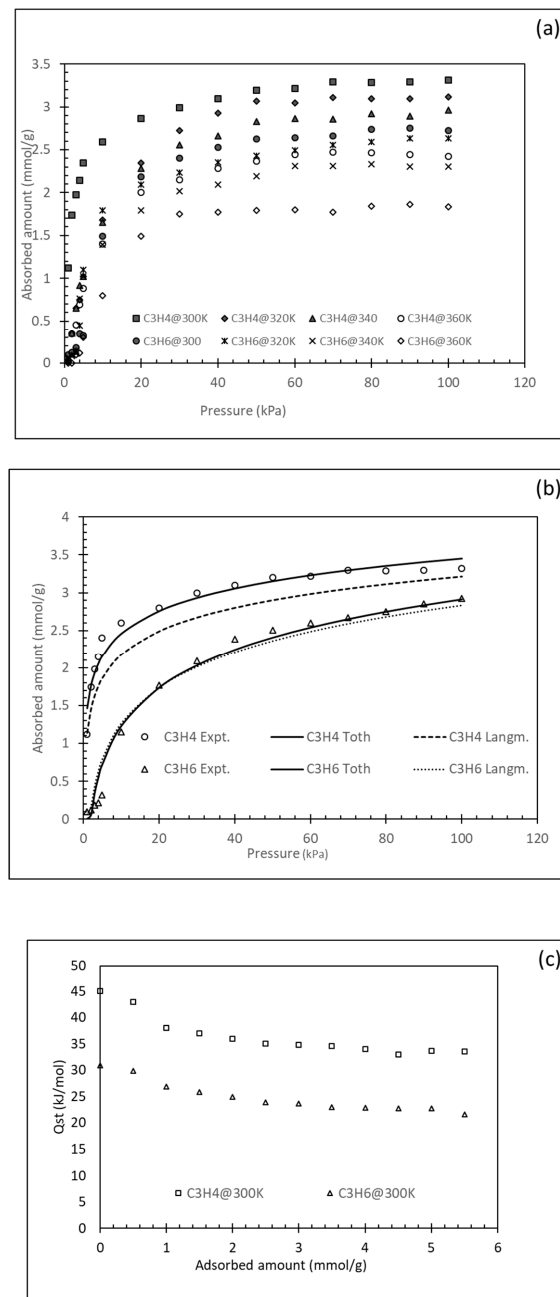


Figure 5. Single gas adsorption. (a) Uptake adsorption amounts at different temperatures and for the two pure propyne and propylene gases; (b) experimental and model fitted isotherms for propyne and propylene at 300 K; (c) isosteric heats of adsorption for propyne and propylene adsorption at 300 K.

Table 2. Reported uptake values of propyne and propylene on metal-organic frameworks (MOFs).

Material	Adsorption Uptake (mmol·g ⁻¹)	Ref	Temp (K)	Pressure (kPa)
	propyne			
SIFSIX-3-Ni	3.32	This study	300	10
SIF-Six-2-Cu-i	1.73	[8]	273	0.1
SIFSIX-3-Ni	2.7	[8]	273	0.1
SIFSIX-1-Cu	0.19	[12]	298	0.1
SIFSIX-2-Cu-i	0.2	[12]	298	0.1
SIFSIX-3-Ni	2.65	[12]	298	0.1
[Cu(dhbc) ₂ (4,4'-bipy)]	0.25	[9]	298	0.1
NK-MOF-Ni	1.83	[8]	273	0.1
NK-MOF-Cu	1.76	[8]	273	0.1

Adsorption isotherms were measured at all temperature ranges, however, only trends obtained at 300 K were reported in Figure 5b for simplicity. Many models are reported in the literature to describe the adsorbent capacity for a certain species. The most commonly used in the case of a gas-solid adsorption system are Langmuir, Freundlich, Sips and Toth isotherms [13]. The first two models are known as the two-parameter models while the later models are a hybrid combination of the two-parameter models. Here only the Langmuir and the Toth are used to fitting the experimental data. The first due to its simplicity and widespread application and the second (Toth) due to its accuracy over a large range of data points and experimental conditions. The Langmuir model assumes monolayer adsorption with similar energy used for all sites on the solid sorbent. In this isotherm, the saturation adsorption capacity is in Equation (1) (Table 3). The two main factors of Equation (1) are estimated from experimental data and used to establish the model fit of the data to the isotherm. The applicability of the isotherm is typically related to another factor that is associated with the Langmuir model as described in Equation (2) (Table 3). The value of the separation factor R_L is indicative of the ability of the model to fit the experimental data. The Toth isotherm [70] (Equation (3), Table 3) is a dual-site isotherm based on the Langmuir and Freundlich isotherms. A value of n close to 1 is an indication of the system heterogeneity; a value of 1 reduced the Toth equation back into Langmuir isotherm. The applicability of this model in a good range of system pressure application resulted in its wider application in gas-solid adsorption systems.

Statistical analyses were used to evaluate the fit of the experimental data to the various models. The most-reported parameter used is based on the average absolute relative deviation (AARD), coefficient of determination (R^2). Experimental data are fitted to isotherms to help predict the general behaviours of the adsorbent adsorbate interactions and uptake values. The system's affinity for adsorption is indicated by the value of the constants calculated. In the case of Langmuir, the linearized form of the Equations (1) and (3) is used to estimate the equilibrium adsorption uptake amount (q_{sat}) under a given pressure and temperature system. It is also related to the maximum adsorbed amount Q . Experimental results obtained for the two gases were analyzed by regression analyses and all model fits are represented in Figure 5b. From the trends shown in Figure 5b, it can be seen that the Langmuir had a varied degree of representation of the system with better presentation of the adsorption of the propylene compared to the propyne system as reflected by lowered AARD (Table 4) for the range of pressures for the case of SIFSIX and propyne systems. The Toth model regression offered a better fit of the experimental data over the entire range of pressures. The representation and fitting of the models are important to estimate the energy in the form of the isosteric heats of adsorption that is based on the Clausius–Clapeyron equation. The calculation of the isosteric heats of adsorption (Q_{st} (kJmol⁻¹)) is essential for the understanding of the strength of the interactions between

the solid surface and the adsorbate in addition to any energetic heterogeneity in the solid surface as given in Equation (5) and Table 3.

Table 3. Mathematical expressions used for the representation of experimental data.

	Equation	Parameter Definition	Equation
Langmuir isotherm	$Q = q_{sat} \frac{k_1 P}{1 + k_1 P}$	Q (mmol·g ⁻¹): adsorption capacity; q _{sat} (mmol·g ⁻¹): equilibrium uptake capacity of the gas species; P: system pressure (kPa); k ₁ : isotherm constant related to the energy of adsorption.	(1)
Separation Factor	$R_l = \frac{1}{1 + k_1 P}$	R _l separation factor	(2)
Toth Isotherm	$Q = q_{sat} \left\{ \left(\frac{(k_1 P)^n}{(1 + k_1 P)^n} \right) \right\}^{\frac{1}{n}}$	k _t and n are Toth constants specific for adsorbate-adsorbent pairs; n indicates the affinity of the adsorption	(3)
average absolute relative deviation	$AARD(100\%) = \frac{100}{N} \sum_{i=1}^N \left \frac{Q_{exp} - Q_{pred}}{Q_{exp}} \right $	Q _{pred} : predicted amounts; Q _{exp} values of Q obtained experimentally; N: number of the experimental data points used in the isotherm fit.	(4)
Isosteric heats of sorption	$Q_{st} = RT^2 \left(\frac{\partial \ln P}{\partial T} \right)_{q_{sat}}$	P: pressure; T: temperatures; q _{sa} : saturated equilibrium uptake amount (mmol·g ⁻¹).	(5)
Purity	$P_{C_3H_6} = \frac{\int_{t_{blowdown}}^{t_{end\ purge}} F_{C_3H_6} dt}{\sum_i \int_{t_{blowdown}}^{t_{end\ purge}} F_i dt}$	F _i : the molar flow rate of component i (C ₃ H ₆ and C ₃ H ₄) (mol s ⁻¹); Q _F : the volumetric flow rate at the bed outlet (m ³ s ⁻¹); F _i = Q _F C _i	(6)
Recovery	$R_{C_3H_6} = \frac{\int_{t_{blowdown}}^{t_{end\ purge}} F_{C_3H_6} dt}{\int_0^{t_{end\ purge}} F_{C_3H_6} dt}$	t: end of purge cycle; Q _F : the volumetric flow rate at the bed outlet (m ³ s ⁻¹)	(7)
Productivity	$Pd_{C_3H_6} = \frac{\int_{t_{blowdown}}^{t_{end\ purge}} F_{C_3H_6} M_{C_3H_6} dt - \int_{t_{rinse}}^{t_{end\ purge}} F_{C_3H_6} M_{C_3H_6} dt}{t_{cycle} m_s}$	M _{CO₂} : the molecular weight of C ₃ H ₆ (kg mol ⁻¹); t _{cycle} : the total time of one repeated cycle (h); [purge, blowdown, rinse]; m _s : the adsorbent mass (kg)	(8)
Power consumption	$E_{VSA} = \int \frac{\gamma}{\gamma-1} \frac{Q_F \varepsilon_{tot} CRT}{\eta} \left[\left(\frac{P_{max}}{P_{min}} \right)^{\frac{\gamma-1}{\gamma}} - 1 \right] dt$	η: the compressor efficiency; γ: the specific heat capacity of the gas, C: the gas concentration (mol m ⁻³); Q _F : the volumetric flow rate at the bed outlet (m ³ s ⁻¹); ε _{tot} : the total bed porosity	(9)

Table 4. Isotherm model fitting parameters.

Parameter	Langmuir		Parameter	Toth	
	C ₃ H ₄	C ₃ H ₆		C ₃ H ₄	C ₃ H ₆
q _{sat} (mmol/g)	3.32	2.93	q _{sat} (mmol/g)	4.09	3.98
k ₁	0.23	0.21	k _t	0.042	0.076
R _l	0.82	0.65	n	0.203	0.019
AARD (%)	13.7	12.2	AARD (%)	0.03	0.04

The isosteric heats of sorption as a function of adsorbed amounts are shown in Figure 5c. At zero uptake, the maximum value of Q_{st} is attained. For SIFSIX and propyne system, the Q_{st} zero was around 45 kJ·Kmol⁻¹ and for propylene system, the maximum value was around 30 kJ·Kmol⁻¹. The higher isosteric heat value is related to the strong interactions between the solid and the gas which is higher for propyne than propylene under the experimental conditions used. In addition, the general trend for all cases is that Q_{st} decreases gradually with the increase in uptake rate of the gases on the pore structure of the solids. The continuous decrease at a similar rate indicates the homogeneity of the pore environment; typically, as Q_{st} increases with higher uptake rates, heterogeneity of the surface is usually present [13]. In addition, the differences between the propyne and propylene are a good indication of the

separation possibilities of the two gases. It can also be inferred that the highest value of Q_{st} was recorded for the lower adsorbate loading (Figure 5c).

3.2. Breakthrough Adsorption

The dynamic breakthrough was established and represented in terms of molar flow rate values vs. operation time in Figure 6a for binary mixtures of C_3H_4/C_3H_6 (30:70 v/v). It can be seen from the trends in Figure 6a that the heavier propylene molecules were eluted first from the column compared to the lighter propyne molecules upon adsorption on SIFSIX-3-Ni. This also confirms earlier findings of the stronger bindings and affinities found between propyne and the SIFSIX adsorbent. The gap showed between the C_3H_4 and C_3H_6 breakthrough lines is a good indication of the ability to separate the two compounds using SIFSIX MOF confirming the potential application of SIFSIX-3-Ni for the separation. Figure 6b gives the temperature histories of the column at the various thermocouple locations (set at the bottom, mid and top of the adsorption vertical column). Around 3500 s, the desorption starts, and a sharp increase in the outlet molar flow rate of the two gases is observed. Figure 6b shows that the temperature increases rapidly at the first stages of operation followed by a return to feed temperature.

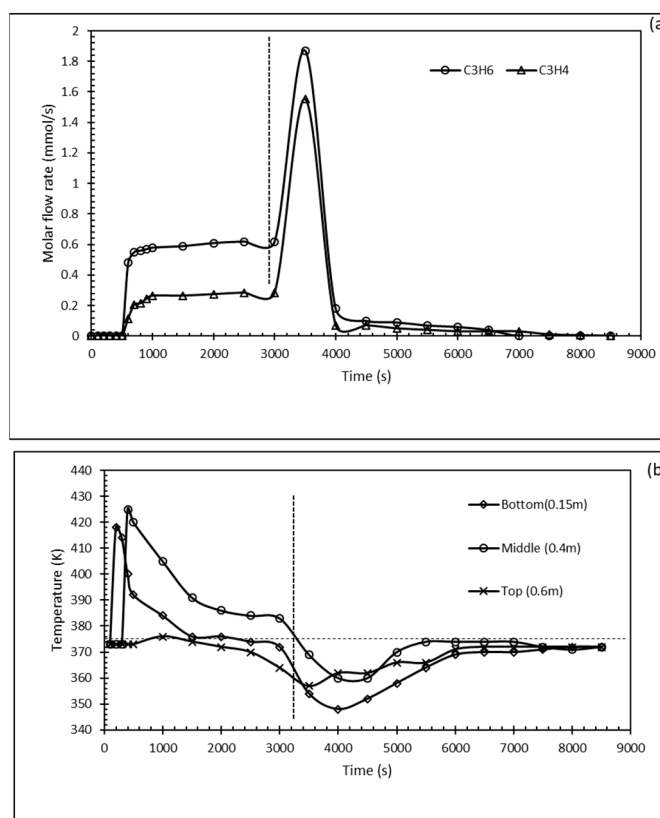


Figure 6. Dynamic breakthrough experiments temperature profile for a multi-component system (30:70% v/v propyne/propylene); (a) molar flow rate with time; (b) temperature profile in the fixed bed column.

3.3. Vacuum Pressure Adsorption (VPA)

For the VSA, the 6-cycle process depicted in Figure 3 was used for the recovery of high purity C_3H_4 and C_3H_6 . The duration of the adsorption (feed) step was set for 800 s followed by a 100 s depressurization. The rinse and purge time were around 600 s while 50 s were used to increase the pressure in the system (Table 1). Four-column VSA units (see Figure 3) were required to continue the feed operation of the system under the given operational conditions. The feed flow rate at each stage was controlled and is given in

Table 1. The pressure change history in the system is given in Figure 7a while the outlet flow rate is depicted in Figure 7b. In the adsorption and depressurization cycle, the C_3H_4 is eluted and the outlet will only have propyne in it. In the rinse stage, no breakthrough of C_3H_6 was observed (Figure 7b). In the blowdown stage, the main constituent of the outlet stream was propylene as well as significant amounts of C_3H_6 leaves the column at the purge stage of the VSA cycle which is recovered to the main propylene stream.

Figure 8 shows the temperature and concentration ($\text{mol}\cdot\text{m}^{-3}$) of gas as obtained at the end of each of the cycles at steady-state conditions. At the end of the adsorption and depressurization operations, the trends can be considered to be similar (Figure 8a,b) to those in Figure 6. It can be seen that the concentration fronts are sharper. Similar observations were made for a cycle of N_2 and C_3H_6 [49]. In the rinse cycle (Figure 8c), the C_3H_6 is fed to the column and C_3H_4 is withdrawn. It can be seen that the system is operated in a way to ensure two-stage fronts of C_3H_6 . Both gases merge near the last stages of the rinse cycle where the cycle is stopped before the breakthrough of C_3H_6 . The temperature is observed to increase towards the last third of the column (Figure 8c). Immediately before the end of the rinse cycle, C_3H_6 is introduced to the column in the blowdown stage (Figure 8d). A slight decrease in C_3H_6 concentration can be seen at the end of the blowdown stage and the subsequent purge stage (Figure 8e). The end of the VSA cycle is the pressurization stage where the column is filled with C_3H_4 .

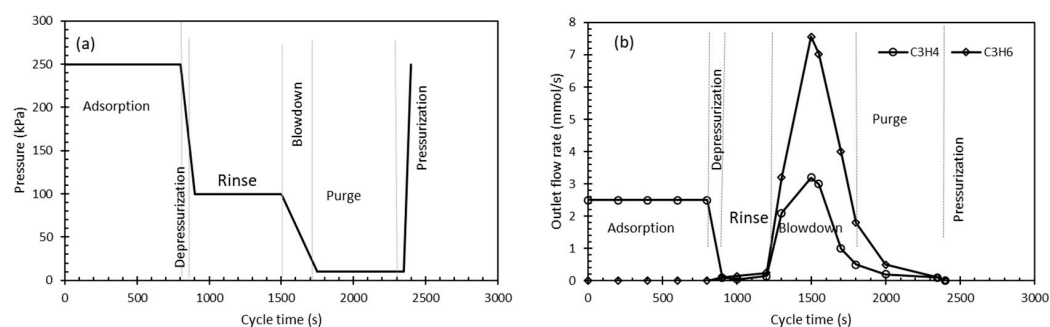


Figure 7. Vacuum swing adsorption (VSA) cycle (a) pressure history in the system; (b) outlet flow rate of profile for a multi-component system (30:70% *v/v* propyne/propylene).

Figure 9 shows the four VSA cycles (as described in Figure 3) represented here as the outlet molar flow rate ($\text{mmol}\cdot\text{s}^{-1}$) with respect to cumulative operation time (min). The figure clearly indicated that cyclic repeatability and consistency was achieved over the four VSA cycles. A very slight variation was noticed only at the start of the first cycle until the system attains its steady-state conditions. Propylene molar flow rate at the beginning of the blowdown stage is at its maximum value before declining with pressure. This steady-state condition and attainment for more than one cycle operation are advantageous. However, purity, productivity and recovery are the most common key indicators used to evaluate the ability of the VSA system to separate the two gases effectively with the required high-grade purity. The mathematical representation of the three indicators is given in Table 3.

The VSA system was tested with respect to changing blowdown time and purge time as indicated in Table 1. In addition, the estimated energy requirements were estimated using Equation (9) (Table 3). In the calculations of the energy consumed, the efficiency of the compressors and the vacuum pump was assumed to be 70%. In reality, the efficiency, especially for the vacuum pump, can be lower but the 70% range is acceptable for calculations and a 72% was reported by Qasem [59]. The calculations were made with the assumptions that the systems attained equilibrium.

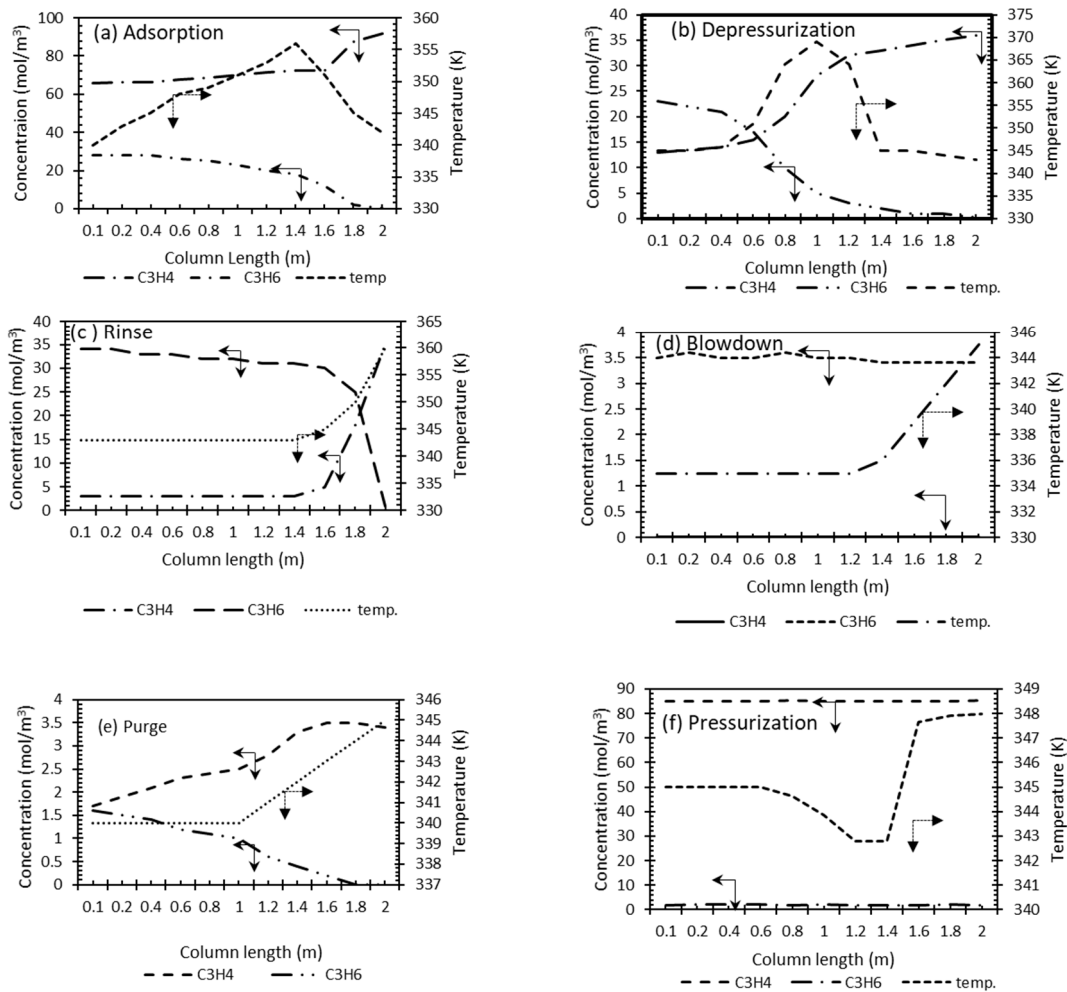


Figure 8. Concentration and temperature history for various stages in VSA column: (a) adsorption (800 s, 250 kPa, 1.2 SLPM) (b) Depressurization (100 s, 100 kPa); (c) rinse (600 s, 100 kPa, 1.2SLPM); (d) blowdown (100 s, 250–10 kPa); (e) purge (600 s, 10 kPa, 1 SLPM); (f) pressurization (50 s, 10–250 kPa, 1.2 SLMP).

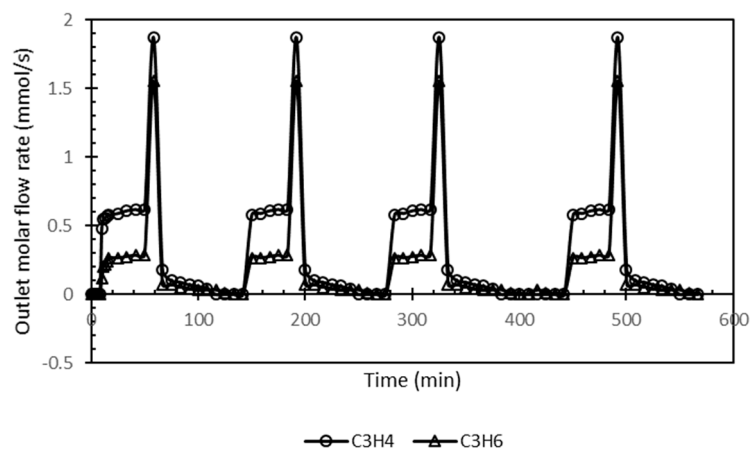


Figure 9. Whole VSA cycle outlet molar flow rate vs. time.

3.4. Energy Consumption, Purity, Recovery and Productivity

Figure 10a,b show the purity and recovery and productivity as a function of different blowdown cycle times. The trends indicate that the longer the blowdown time the higher the C₃H₆ recovery but on the account of decreasing purity. Accordingly, a trade-off time

can be selected (shorter time of 100 s) which was deemed suitable for operation in the VSA cycles. This is well supported by the productivity trend (Figure 10b) that supports a shorter blowdown time (100 s) where the productivity value was highest. Figure 10c represents the changes of purity and recovery with respect to the purge cycle time (600–750 s) while Figure 10d depicts the impact of the changing productivity with respect to change in purge time. The increase in purge time had a positive effect on C_3H_6 recovery but reduced productivity and recovery. Accordingly, under the experimental conditions used in this study for VSA, the purge time of 600 s was considered a suitable trade-off time for purging. Figure 10e,f shows the power consumption used in the VSA system under consideration with respect to the changes in purge and blowdown time respectively. The increase in the blow downtime (at 600 s Purge) resulted in nearly the same energy consumption requirement. On the other hand, a vast difference was noticed in the energy requirements when the purge time increased from 600 to 750 at a blowdown time of 100 s. Although the amount of desorbed C_3H_6 was not changed with the prolonged purge time, the overall time for the completion of the VSA will change in addition to the energy requirements. Recovery up to 99%, purity of 98.5% were achieved at a purge time of 600 s. Maximum achieved purity and recovery were 97.4% and 98.5% at 100 s blowdown time. Energy and power consumption varied between 63–70 kWh/ton at the range of purge and blowdown time used. The times given here were suitable for use with the bed dimensions and in agreement with those suggested in other studies [52]. A much shorter purge time was reported for a CO_2 and N_2 separation system where the blowdown time was 100 s and purge time was changed between 50–150 s [38,59,73]. The smaller reported purge time was consistent with the small adsorption bed that has a length of 0.07 m and an inner diameter of 0.4 cm. The bigger columns in addition to the times employed in this study are in more agreement with scaled-down industrial application cycles and represent more realistic operating conditions.

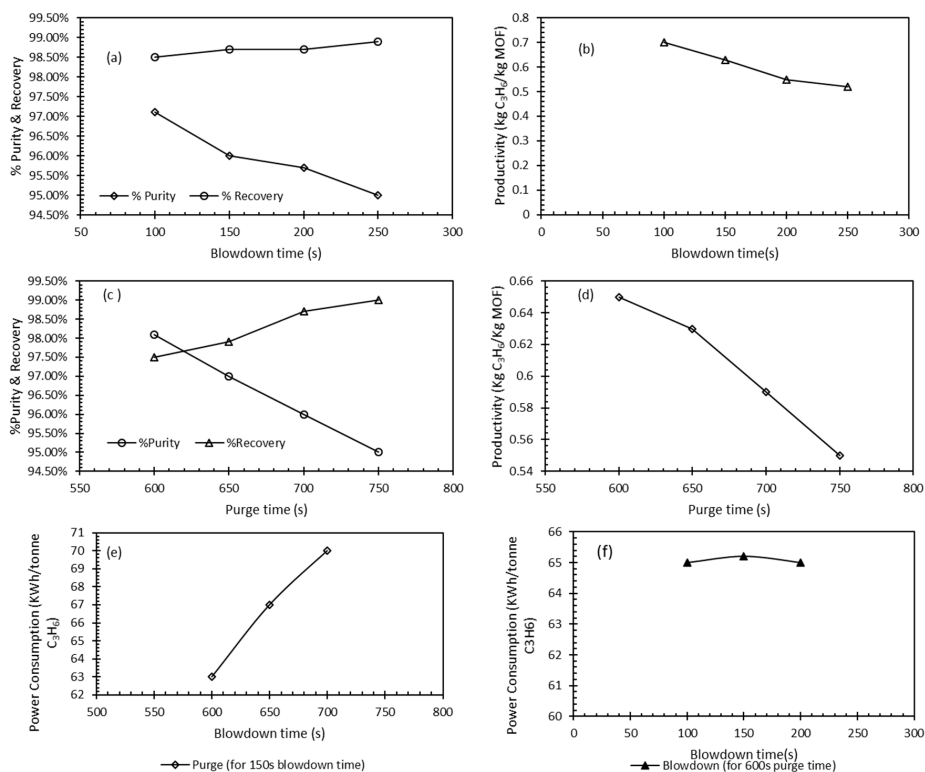


Figure 10. Key VSA performance indicators for C_3H_4/C_3H_6 separation: (a) impact of blowdown time on purity and recovery of C_3H_6 ; (b) productivity with respect to blowdown time for C_3H_6 ; (c) purity and recovery as a function of purge time; (d) productivity of C_3H_6 with change in purge time; (e) power consumption with respect to different blowdown times and purge of 150 s; (f) power consumption as a function of blowdown time for 600 s purge time.

4. Conclusions

In this work benchmark SIFSIX-3-Ni uptake removal of C_3H_4 from a stream of C_3H_6 was achieved with a value of $3.32 \text{ mmol}\cdot\text{g}^{-1}$ under the experimental conditions and set us used in this study. Toth mathematical isotherm represented the adsorption data well over the full range of pressures and for both gases. High isosteric heats of adsorption were obtained for propyne ($45 \text{ kJ}\cdot\text{Kmol}^{-1}$) compared to around $30 \text{ kJ}\cdot\text{Kmol}^{-1}$ for propylene indicating a strong affinity for the C_3H_4 on the MOF. Breakthrough experiments ascertained the ability of the MOF to separate the two materials with the heaviest molecule being eluded first from the top of the fixed bed. 6-step vacuum pressure swing adsorption process was used to develop and test the separation under real industrial conditions to facilitate the understanding of the performance and effectiveness of MOF for the C_3H_4/C_3H_6 separation. C_3H_6 can be successfully separated under controlled VSA cycle conditions with the best purity, recovery and productivity at blow downtime of 100 s and a purge time of 600 s. At such conditions, recovery up to 99%, purity of 98.5% were achieved. While a maximum achieved purity and recovery were 97.4% and 98.5% at 100 s blowdown time. Energy and power consumption varied between 63–70 kWh/ton at the range of purge and blowdown time used.

Supplementary Materials: The following are available online at <https://www.mdpi.com/1996-1073/14/3/609/s1>, Figure S1: Schematic of High-pressure magnetic suspension (Rubotherm), Figure S2: The 6 steps of the VSA cycle, Figure S3: Characterization of the prepared SIFSIX-3-Ni (a) XRD and (b) FTIR, Figure S4: TGA mass loss with respect of temperature for the SIFSIX-3-Ni, Figure S5: N_2 adsorption desorption, Figure S6: Adsorption and desorption of propylene and propyne at 300 K.

Author Contributions: Conceptualization, Methodology, Modeling, Figures preparation, software, pre-Writing-Original draft preparation and experimental trial, M.K.; data manipulation, kinetics Data curation, Discussion, Validation, Tables preparation Writing-Reviewing and Editing, F.A.; Conceptualization, Methodology, Modeling, Figures preparation, software, pre-Writing-Original draft preparation, G.W. All authors have read and agreed to the published version of the manuscript.

Funding: This research was funded by a grant from the Qatar National Research Fund (QNRF) under the National Priorities Research Program award number NPRP10-0107-170119. And the APC was funded by QNRF fund award number NPRP10-0107-170119.

Acknowledgments: The work was made possible by a grant from the Qatar National Research Fund (QNRF) under the National Priorities Research Program award number NPRP10-0107-170119. Its content is solely the responsibility of the authors and does not necessarily represent the official views of QNRF. The authors would like to acknowledge the CLU labs at Qatar University. The APC was funded by QNRF fund award number NPRP10-0107-170119.

Conflicts of Interest: The authors declare no conflict of interest.

References

1. Ashok, A.; Kumar, A.; Bhosale, R.; Saad, M.A.S.; AlMomani, F.; Tarlochan, F. Study of ethanol dehydrogenation reaction mechanism for hydrogen production on combustion synthesized cobalt catalyst. *Int. J. Hydrogen Energy* **2017**, *42*, 23464–23473. [[CrossRef](#)]
2. Mundstock, A.; Wang, N.; Friebe, S.; Caro, J. Propane/propene permeation through Na-X membranes: The interplay of separation performance and pre-synthetic support functionalization. *Microporous Mesoporous Mater.* **2015**, *215*, 20–28. [[CrossRef](#)]
3. Martins, V.F.; Seabra, R.; Silva, P.; Ribeiro, A.M.; Cho, K.H.; Lee, U.-H.; Chang, J.-S.; Loureiro, J.M.; Rodrigues, A.E.; Ferreira, A. C2/C3 Hydrocarbon Separation by Pressure Swing Adsorption on MIL-100 (Fe). *Ind. Eng. Chem. Res.* **2020**, *59*, 10568–10582. [[CrossRef](#)]
4. Lan, T.; Li, L.; Chen, Y.; Wang, X.; Yang, J.; Li, J. Opportunities and critical factors of porous metal–organic frameworks for industrial light olefins separation. *Mater. Chem. Front.* **2020**, *4*, 1954–1984. [[CrossRef](#)]
5. Yang, R.; Gao, R.; Qian, Z.; Wang, Y. Batch and fixed bed column selective adsorption of C6, C8 and C10 linear α -olefins from binary liquid olefin/paraffin mixtures onto 5A and 13X microporous molecular sieves. *Sep. Purif. Technol.* **2020**, *230*, 115884. [[CrossRef](#)]
6. Andrade, M.; Relvas, F.; Mendes, A. Highly propylene equilibrium selective carbon molecular sieve adsorbent. *Sep. Purif. Technol.* **2020**, *245*, 116853. [[CrossRef](#)]

7. Tran, N.T.; Kim, J.; Othman, M.R. Microporous ZIF-8 and ZIF-67 membranes grown on mesoporous alumina substrate for selective propylene transport. *Sep. Purif. Technol.* **2020**, *233*, 116026. [[CrossRef](#)]
8. Li, L.; Guo, L.; Zheng, F.; Zhang, Z.; Yang, Q.; Yang, Y.; Ren, Q.; Bao, Z. Calcium-Based Metal–Organic Framework for Simultaneous Capture of Trace Propyne and Propadiene from Propylene. *ACS Appl. Mater. Interfaces* **2020**, *12*, 17147–17154. [[CrossRef](#)] [[PubMed](#)]
9. Li, L.; Krishna, R.; Wang, Y.; Yang, J.; Wang, X.; Li, J. Exploiting the gate opening effect in a flexible MOF for selective adsorption of propyne from C1/C2/C3 hydrocarbons. *J. Mater. Chem. A* **2016**, *4*, 751–755. [[CrossRef](#)]
10. Yang, L.; Cui, X.; Zhang, Y.; Yang, Q.; Xing, H. A highly sensitive flexible metal–organic framework sets a new benchmark for separating propyne from propylene. *J. Mater. Chem. A* **2018**, *6*, 24452–24458. [[CrossRef](#)]
11. Peng, Y.L.; He, C.; Pham, T.; Wang, T.; Li, P.; Krishna, R.; Forrest, K.A.; Hogan, A.; Suepaul, S.; Space, B. Robust microporous metal–organic frameworks for highly efficient and simultaneous removal of propyne and propadiene from propylene. *Angew. Chemie Int. Ed.* **2019**, *58*, 10209–10214. [[CrossRef](#)] [[PubMed](#)]
12. Yang, L.; Cui, X.; Yang, Q.; Qian, S.; Wu, H.; Bao, Z.; Zhang, Z.; Ren, Q.; Zhou, W.; Chen, B. A Single-Molecule Propyne Trap: Highly Efficient Removal of Propyne from Propylene with Anion-Pillared Ultramicroporous Materials. *Adv. Mater.* **2018**, *30*, 1705374. [[CrossRef](#)] [[PubMed](#)]
13. Abedini, H.; Shariati, A.; Khosravi-Nikou, M.R. Adsorption of propane and propylene on M-MOF-74 (M=Cu, Co): Equilibrium and kinetic study. *Chem. Eng. Res. Des.* **2020**, *153*, 96–106. [[CrossRef](#)]
14. Da Silva, F.A.; Rodrigues, A.E. Adsorption equilibria and kinetics for propylene and propane over 13X and 4A zeolite pellets. *Ind. Eng. Chem. Res.* **1999**, *38*, 2051–2057. [[CrossRef](#)]
15. Jorge, M.; Lamia, N.; Rodrigues, A.E. Molecular simulation of propane/propylene separation on the metal–organic framework CuBTC. *Colloids Surfaces A Physicochem. Eng. Asp.* **2010**, *357*, 27–34. [[CrossRef](#)]
16. Lamia, N.; Wolff, L.; Leflaive, P.; Sá Gomes, P.; Grande, C.A.; Rodrigues, A.E. Propane/propylene separation by simulated moving bed I. Adsorption of propane, propylene and isobutane in pellets of 13X zeolite. *Sep. Sci. Technol.* **2007**, *42*, 2539–2566. [[CrossRef](#)]
17. Martins, V.F.D.; Ribeiro, A.M.; Plaza, M.G.; Santos, J.C.; Loureiro, J.M.; Ferreira, A.F.P.; Rodrigues, A.E. Gas-phase simulated moving bed: Propane/propylene separation on 13X zeolite. *J. Chromatogr. A* **2015**, *1423*, 136–148. [[CrossRef](#)]
18. Plaza, M.G.; Ribeiro, A.M.; Ferreira, A.; Santos, J.C.; Lee, U.H.; Chang, J.-S.; Loureiro, J.M.; Rodrigues, A.E. Propylene/propane separation by vacuum swing adsorption using Cu-BTC spheres. *Sep. Purif. Technol.* **2012**, *90*, 109–119. [[CrossRef](#)]
19. Wang, S.; Zhang, Y.; Tang, Y.; Wen, Y.; Lv, Z.; Liu, S.; Li, X.; Zhou, X. Propane-selective design of zirconium-based MOFs for propylene purification. *Chem. Eng. Sci.* **2020**, *219*, 115604. [[CrossRef](#)]
20. Das, M.C.; Guo, Q.; He, Y.; Kim, J.; Zhao, C.-G.; Hong, K.; Xiang, S.; Zhang, Z.; Thomas, K.M.; Krishna, R. Interplay of metalloligand and organic ligand to tune micropores within isostructural mixed-metal organic frameworks (M' MOFs) for their highly selective separation of chiral and achiral small molecules. *J. Am. Chem. Soc.* **2012**, *134*, 8703–8710. [[CrossRef](#)]
21. Li, L.; Lin, R.-B.; Krishna, R.; Wang, X.; Li, B.; Wu, H.; Li, J.; Zhou, W.; Chen, B. Flexible–robust metal–organic framework for efficient removal of propyne from propylene. *J. Am. Chem. Soc.* **2017**, *139*, 7733–7736. [[CrossRef](#)] [[PubMed](#)]
22. Li, L.; Wen, H.M.; He, C.; Lin, R.B.; Krishna, R.; Wu, H.; Zhou, W.; Li, J.; Li, B.; Chen, B. A metal–organic framework with suitable pore size and specific functional sites for the removal of trace propyne from propylene. *Angew. Chemie* **2018**, *130*, 15403–15408. [[CrossRef](#)]
23. Wang, X.; Krishna, R.; Li, L.; Wang, B.; He, T.; Zhang, Y.-Z.; Li, J.-R.; Li, J. Guest-dependent pressure induced gate-opening effect enables effective separation of propene and propane in a flexible MOF. *Chem. Eng. J.* **2018**, *346*, 489–496. [[CrossRef](#)]
24. Elsaïdi, S.K.; Mohamed, M.H.; Banerjee, D.; Thallapally, P.K. Flexibility in Metal–Organic Frameworks: A fundamental understanding. *Coord. Chem. Rev.* **2018**, *358*, 125–152. [[CrossRef](#)]
25. Zhang, J.; Chen, Z. Metal-organic frameworks as stationary phase for application in chromatographic separation. *J. Chromatogr. A* **2017**, *1530*, 1–18. [[CrossRef](#)] [[PubMed](#)]
26. Saha, D.; Bao, Z.; Jia, F.; Deng, S. Adsorption of CO₂, CH₄, N₂O, and N₂ on MOF-5, MOF-177, and zeolite 5A. *Environ. Sci. Technol.* **2010**, *44*, 1820–1826. [[CrossRef](#)]
27. Grande, C.A.; Gascon, J.; Kapteijn, F.; Rodrigues, A.E. Propane/propylene separation with Li-exchanged zeolite 13X. *Chem. Eng. J.* **2010**, *160*, 207–214. [[CrossRef](#)]
28. Silva, F.A.D.; Rodrigues, A.E. Propylene/propane separation by vacuum swing adsorption using 13X zeolite. *AIChE J.* **2001**, *47*, 341–357. [[CrossRef](#)]
29. Madden, D.; Albadarin, A.B.; O’Nolan, D.; Cronin, P.; Perry IV, J.J.; Solomon, S.; Curtin, T.; Khraisheh, M.; Zaworotko, M.J.; Walker, G.M. Metal-Organic Material Polymer Coatings for Enhanced Gas Sorption Performance and Hydrolytic Stability Under Humid Conditions. *ACS Appl. Mater. Interfaces* **2020**. [[CrossRef](#)]
30. Mukherjee, S.; Zaworotko, M.J. Crystal Engineering of Hybrid Coordination Networks: From Form to Function. *Trends Chem.* **2020**, *2*, 506–518. [[CrossRef](#)]
31. Li, L.; Duan, Y.; Liao, S.; Ke, Q.; Qiao, Z.; Wei, Y. Adsorption and separation of propane/propylene on various ZIF-8 polymorphs: Insights from GCMC simulations and the ideal adsorbed solution theory (IAST). *Chem. Eng. J.* **2020**, *386*, 123945. [[CrossRef](#)]
32. Dhoke, C.; Cloete, S.; Krishnamurthy, S.; Seo, H.; Luz, I.; Soukri, M.; Park, Y.-k.; Blom, R.; Amini, S.; Zaabout, A. Sorbents screening for post-combustion CO₂ capture via combined temperature and pressure swing adsorption. *Chem. Eng. J.* **2020**, *380*, 122201. [[CrossRef](#)]

33. Ben-Mansour, R.; Qasem, N.A.A.; Antar, M.A. Carbon dioxide adsorption separation from dry and humid CO₂/N₂ mixture. *Comput. Chem. Eng.* **2018**, *117*, 221–235. [[CrossRef](#)]
34. Ben-Mansour, R.; Bamidele, O.; Habib, M. Evaluation of Mg-MOF-74 for post-combustion carbon dioxide capture through pressure swing adsorption. *Int. J. Energy Res.* **2015**, *39*, 1994–2007. [[CrossRef](#)]
35. Karra, J.R.; Grabicka, B.E.; Huang, Y.-G.; Walton, K.S. Adsorption study of CO₂, CH₄, N₂, and H₂O on an interwoven copper carboxylate metal–organic framework (MOF-14). *J. Colloid Interface Sci.* **2013**, *392*, 331–336. [[CrossRef](#)]
36. Vikrant, K.; Kim, K.-H.; Kumar, V.; Giannakoudakis, D.A.; Boukhvalov, D.W. Adsorptive removal of an eight-component volatile organic compound mixture by Cu-, Co-, and Zr-metal-organic frameworks: Experimental and theoretical studies. *Chem. Eng. J.* **2020**, *397*, 125391. [[CrossRef](#)]
37. Wang, C.; Liu, X.; Li, W.; Huang, X.; Luan, S.; Hou, X.; Zhang, M.; Wang, Q. CO₂ mediated fabrication of hierarchically porous metal-organic frameworks. *Microporous Mesoporous Mater.* **2019**, *277*, 154–162. [[CrossRef](#)]
38. Qasem, N.A.A.; Ben-Mansour, R.; Habib, M.A. An efficient CO₂ adsorptive storage using MOF-5 and MOF-177. *Appl. Energy* **2018**, *210*, 317–326. [[CrossRef](#)]
39. Bahamon, D.; Díaz-Márquez, A.; Gamallo, P.; Vega, L.F. Energetic evaluation of swing adsorption processes for CO₂ capture in selected MOFs and zeolites: Effect of impurities. *Chem. Eng. J.* **2018**, *342*, 458–473. [[CrossRef](#)]
40. Ahmad, M.Z.; Navarro, M.; Lhotka, M.; Zornoza, B.; Téllez, C.; de Vos, W.M.; Benes, N.E.; Konnertz, N.M.; Visser, T.; Semino, R.; et al. Enhanced gas separation performance of 6FDA-DAM based mixed matrix membranes by incorporating MOF UiO-66 and its derivatives. *J. Membr. Sci.* **2018**, *558*, 64–77. [[CrossRef](#)]
41. Fischer, M.; Hoffmann, F.; Fröba, M. Molecular simulation of hydrogen adsorption in metal-organic frameworks. *Colloids Surfaces A Physicochem. Eng. Asp.* **2010**, *357*, 35–42. [[CrossRef](#)]
42. Yin, N.; Wang, K.; Xia, Y.A.; Li, Z. Novel melamine modified metal-organic frameworks for remarkably high removal of heavy metal Pb (II). *Desalination* **2018**, *430*, 120–127. [[CrossRef](#)]
43. Kumar, A.; Hua, C.; Madden, D.G.; O’Nolan, D.; Chen, K.-J.; Keane, L.-A.J.; Perry, J.J.; Zaworotko, M.J. Hybrid ultramicroporous materials (HUMs) with enhanced stability and trace carbon capture performance. *Chem. Commun.* **2017**, *53*, 5946–5949. [[CrossRef](#)]
44. Khraisheh, M.; Mukherjee, S.; Kumar, A.; Al Momani, F.; Walker, G.; Zaworotko, M.J. An overview on trace CO₂ removal by advanced physisorbent materials. *J. Environ. Manag.* **2020**, *255*, 109874. [[CrossRef](#)] [[PubMed](#)]
45. Lin, Z.-T.; Liu, Q.-Y.; Yang, L.; He, C.-T.; Li, L.; Wang, Y.-L. Fluorinated Biphenyldicarboxylate-Based Metal–Organic Framework Exhibiting Efficient Propyne/Propylene Separation. *Inorganic Chem.* **2020**, *59*, 4030–4036. [[CrossRef](#)]
46. Wen, H.-M.; Li, L.; Lin, R.-B.; Li, B.; Hu, B.; Zhou, W.; Hu, J.; Chen, B. Fine-tuning of nano-traps in a stable metal–organic framework for highly efficient removal of propyne from propylene. *J. Mater. Chem. A* **2018**, *6*, 6931–6937. [[CrossRef](#)]
47. Park, J.; Lively, R.P.; Sholl, D.S. Establishing upper bounds on CO₂ swing capacity in sub-ambient pressure swing adsorption via molecular simulation of metal–organic frameworks. *J. Mater. Chem. A* **2017**, *5*, 12258–12265. [[CrossRef](#)]
48. Guang, C.; Zhao, X.; Zhang, Z.; Gao, J.; Li, M. Optimal design and performance enhancement of heteroazeotropic and pressure-swing coupling distillation for downstream isopropanol separation. *Sep. Purif. Technol.* **2020**, *242*, 116836. [[CrossRef](#)]
49. Ribeiro, A.M.; Campo, M.C.; Narin, G.; Santos, J.C.; Ferreira, A.; Chang, J.-S.; Hwang, Y.K.; Seo, Y.-K.; Lee, U.-H.; Loureiro, J.M. Pressure swing adsorption process for the separation of nitrogen and propylene with a MOF adsorbent MIL-100 (Fe). *Sep. Purif. Technol.* **2013**, *110*, 101–111. [[CrossRef](#)]
50. Da Silva, F.A.; Rodrigues, A.E. Propylene/propane separation by pressure swing adsorption. In *Adsorption Science and Technology*; World Scientific: Singapore, 2000; pp. 537–541.
51. Hedim, N.; Andersson, L.; Bergström, L.; Yan, J. Adsorbents for the post-combustion capture of CO₂ using rapid temperature swing or vacuum swing adsorption. *Appl. Energy* **2013**, *104*, 418–433. [[CrossRef](#)]
52. Dasgupta, S.; Biswas, N.; Gode, N.G.; Divekar, S.; Nanoti, A.; Goswami, A.N. CO₂ recovery from mixtures with nitrogen in a vacuum swing adsorber using metal organic framework adsorbent: A comparative study. *Int. J. Greenh. Gas Control* **2012**, *7*, 225–229. [[CrossRef](#)]
53. Pai, K.N.; Baboolal, J.D.; Sharp, D.A.; Rajendran, A. Evaluation of diamine-appended metal-organic frameworks for post-combustion CO₂ capture by vacuum swing adsorption. *Sep. Purif. Technol.* **2019**, *211*, 540–550. [[CrossRef](#)]
54. Mofarahi, M.; Sadrameli, M.; Towfighi, J. Four-bed vacuum pressure swing adsorption process for propylene/propane separation. *Ind. Eng. Chem. Res.* **2005**, *44*, 1557–1564. [[CrossRef](#)]
55. Maring, B.J.; Webley, P.A. A new simplified pressure/vacuum swing adsorption model for rapid adsorbent screening for CO₂ capture applications. *Int. J. Greenh. Gas Control* **2013**, *15*, 16–31. [[CrossRef](#)]
56. Burns, T.D.; Pai, K.N.; Subraveti, S.G.; Collins, S.P.; Krykunov, M.; Rajendran, A.; Woo, T.K. Prediction of MOF Performance in Vacuum Swing Adsorption Systems for Postcombustion CO₂ Capture Based on Integrated Molecular Simulations, Process Optimizations, and Machine Learning Models. *Environ. Sci. Technol.* **2020**, *54*, 4536–4544. [[CrossRef](#)] [[PubMed](#)]
57. Ben-Mansour, R.; Qasem, N.A.A. An efficient temperature swing adsorption (TSA) process for separating CO₂ from CO₂/N₂ mixture using Mg-MOF-74. *Energy Convers. Manag.* **2018**, *156*, 10–24. [[CrossRef](#)]
58. Sinha, A.; Darunte, L.A.; Jones, C.W.; Realf, M.J.; Kawajiri, Y. Systems Design and Economic Analysis of Direct Air Capture of CO₂ through Temperature Vacuum Swing Adsorption Using MIL-101 (Cr)-PEI-800 and mmen-Mg-2 (dobpdc) MOF Adsorbents (vol 56, pg 750, 2017). *Ind. Eng. Chem. Res.* **2020**, *59*, 503–505. [[CrossRef](#)]

59. Qasem, N.A.; Ben-Mansour, R. Energy and productivity efficient vacuum pressure swing adsorption process to separate CO₂ from CO₂/N₂ mixture using Mg-MOF-74: A CFD simulation. *Appl. Energy* **2018**, *209*, 190–202. [[CrossRef](#)]
60. Du, W.; Alkebsi, K.A.M. Model Predictive Control and Optimization of Vacuum Pressure Swing Adsorption for Carbon Dioxide Capture. In Proceedings of the 2017 6th International Symposium on Advanced Control of Industrial Processes (AdCONIP), Taipei, Taiwan, 28–31 May 2017; pp. 412–417.
61. Durán, I.; Rubiera, F.; Pevida, C. Vacuum swing CO₂ adsorption cycles in Waste-to-Energy plants. *Chem. Eng. J.* **2020**, *382*, 122841. [[CrossRef](#)]
62. Elsaidi, S.K.; Mohamed, M.H.; Schaef, H.T.; Kumar, A.; Lusi, M.; Pham, T.; Forrest, K.A.; Space, B.; Xu, W.; Halder, G.J. Hydrophobic pillared square grids for selective removal of CO₂ from simulated flue gas. *Chem. Commun.* **2015**, *51*, 15530–15533. [[CrossRef](#)]
63. Khraisheh, M.; Almomani, F.; Walker, G. Solid Sorbents as a Retrofit Technology for CO₂ Removal from Natural Gas Under High Pressure and Temperature Conditions. *Sci. Rep.* **2020**, *10*, 269. [[CrossRef](#)] [[PubMed](#)]
64. Madden, D.G.; O’Nolan, D.; Chen, K.-J.; Hua, C.; Kumar, A.; Pham, T.; Forrest, K.A.; Space, B.; Perry, J.J.; Khraisheh, M. Highly selective CO₂ removal for one-step liquefied natural gas processing by physisorbents. *Chem. Commun.* **2019**, *55*, 3219–3222. [[CrossRef](#)] [[PubMed](#)]
65. Maruyama, R.T.; Pai, K.N.; Subraveti, S.G.; Rajendran, A. Improving the performance of vacuum swing adsorption based CO₂ capture under reduced recovery requirements. *Int. J. Greenh. Gas Control* **2020**, *93*, 102902. [[CrossRef](#)]
66. Plaza, M.; Ferreira, A.; Santos, J.; Ribeiro, A.; Müller, U.; Trukhan, N.; Loureiro, J.; Rodrigues, A. Propane/propylene separation by adsorption using shaped copper trimesate MOF. *Microporous Mesoporous Mater.* **2012**, *157*, 101–111. [[CrossRef](#)]
67. Bhatt, P.M.; Belmabkhout, Y.; Cadiou, A.; Adil, K.; Shekhah, O.; Shkurenko, A.; Barbour, L.J.; Eddaoudi, M. A fine-tuned fluorinated MOF addresses the needs for trace CO₂ removal and air capture using physisorption. *J. Am. Chem. Soc.* **2016**, *138*, 9301–9307. [[CrossRef](#)]
68. Kumar, A.; Madden, D.G.; Lusi, M.; Chen, K.J.; Daniels, E.A.; Curtin, T.; Perry IV, J.J.; Zaworotko, M.J. Direct air capture of CO₂ by physisorbent materials. *Angew. Chemie Int. Ed.* **2015**, *54*, 14372–14377. [[CrossRef](#)]
69. Ullah, S.; Bustam, M.A.; Al-Sehemi, A.G.; Assiri, M.A.; Abdul Kareem, F.A.; Mukhtar, A.; Ayoub, M.; Gonfa, G. Influence of post-synthetic graphene oxide (GO) functionalization on the selective CO₂/CH₄ adsorption behavior of MOF-200 at different temperatures; an experimental and adsorption isotherms study. *Microporous Mesoporous Mater.* **2020**, *296*, 110002. [[CrossRef](#)]
70. Ullah, S.; Bustam, M.A.; Assiri, M.A.; Al-Sehemi, A.G.; Gonfa, G.; Mukhtar, A.; Abdul Kareem, F.A.; Ayoub, M.; Saqib, S.; Mellon, N.B. Synthesis and characterization of mesoporous MOF UMCM-1 for CO₂/CH₄ adsorption; an experimental, isotherm modeling and thermodynamic study. *Microporous Mesoporous Mater.* **2020**, *294*, 109844. [[CrossRef](#)]
71. Ullah, S.; Bustam, M.A.; Assiri, M.A.; Al-Sehemi, A.G.; Sagir, M.; Abdul Kareem, F.A.; Elkhalfah, A.E.I.; Mukhtar, A.; Gonfa, G. Synthesis, and characterization of metal-organic frameworks -177 for static and dynamic adsorption behavior of CO₂ and CH₄. *Microporous Mesoporous Mater.* **2019**, *288*, 109569. [[CrossRef](#)]
72. Li, L.; Lin, R.-B.; Wang, X.; Zhou, W.; Jia, L.; Li, J.; Chen, B. Kinetic separation of propylene over propane in a microporous metal-organic framework. *Chem. Eng. J.* **2018**, *354*, 977–982. [[CrossRef](#)]
73. Qasem, N.A.A.; Ben-Mansour, R. Adsorption breakthrough and cycling stability of carbon dioxide separation from CO₂/N₂/H₂O mixture under ambient conditions using 13X and Mg-MOF-74. *Appl. Energy* **2018**, *230*, 1093–1107. [[CrossRef](#)]